

## Effects of Conformal Nanoscale Coatings on Thermal Performance of Vertically Aligned Carbon Nanotubes

Silvestri, Cinzia; Riccio, Michele; Poelma, Rene H.; Jovic, Aleksandar; Morana, Bruno; Vollebregt, Sten; Irace, Andrea; Zhang, Guo Qi; Sarro, Pasqualina M.

**DOI**

[10.1002/smll.201800614](https://doi.org/10.1002/smll.201800614)

**Publication date**

2018

**Document Version**

Final published version

**Published in**

Small

**Citation (APA)**

Silvestri, C., Riccio, M., Poelma, R. H., Jovic, A., Morana, B., Vollebregt, S., Irace, A., Zhang, G. Q., & Sarro, P. M. (2018). Effects of Conformal Nanoscale Coatings on Thermal Performance of Vertically Aligned Carbon Nanotubes. *Small*, 14(20), 1-10. <https://doi.org/10.1002/smll.201800614>

**Important note**

To cite this publication, please use the final published version (if applicable).  
Please check the document version above.

**Copyright**

Other than for strictly personal use, it is not permitted to download, forward or distribute the text or part of it, without the consent of the author(s) and/or copyright holder(s), unless the work is under an open content license such as Creative Commons.

**Takedown policy**

Please contact us and provide details if you believe this document breaches copyrights.  
We will remove access to the work immediately and investigate your claim.

***Green Open Access added to TU Delft Institutional Repository***

***'You share, we take care!' – Taverne project***

**<https://www.openaccess.nl/en/you-share-we-take-care>**

# Effects of Conformal Nanoscale Coatings on Thermal Performance of Vertically Aligned Carbon Nanotubes

Cinzia Silvestri,\* Michele Riccio, René H. Poelma, Aleksandar Jovic, Bruno Morana, Sten Vollebregt, Andrea Irace, Guo Qi Zhang, and Pasqualina M. Sarro\*

The high aspect ratio and the porous nature of spatially oriented forest-like carbon nanotube (CNT) structures represent a unique opportunity to engineer a novel class of nanoscale assemblies. By combining CNTs and conformal coatings, a 3D lightweight scaffold with tailored behavior can be achieved. The effect of nanoscale coatings, aluminum oxide ( $\text{Al}_2\text{O}_3$ ) and nonstoichiometric amorphous silicon carbide (a-SiC), on the thermal transport efficiency of high aspect ratio vertically aligned CNTs, is reported herein. The thermal performance of the CNT-based nanostructure strongly depends on the achieved porosity, the coating material and its infiltration within the nanotube network. An unprecedented enhancement in terms of effective thermal conductivity in a-SiC coated CNTs has been obtained: 181% compared to the as-grown CNTs and  $\text{Al}_2\text{O}_3$  coated CNTs. Furthermore, the integration of coated high aspect ratio CNTs in an epoxy molding compound demonstrates that, next to the required thermal conductivity, the mechanical compliance for thermal interface applications can also be achieved through coating infiltration into foam-like CNT forests.

1D nanostructures such as nanotubes, nanowires, and vertical core-shell heterostructures are attractive building block materials to improve performance in various applications, including electronic and optoelectronic devices,<sup>[1–3]</sup> electrophysiological signal detection,<sup>[4,5]</sup> energy storage, and conversion.<sup>[6,7]</sup> The formation of high-density and spatially oriented forest-like nanostructures is central in many of the mentioned applications due to a significantly increased surface-to-volume ratio in comparison to conventional bulk materials. Additionally, the bottom-up approach, often used to achieve those nanostructure clusters, allows to control their localized growth, their aspect ratio, and

can be compatible with large area processes depending on the synthesis and patterning process.

Recently, great effort has been devoted to create and to engineer a novel class of multiscale macroscopic composite materials, which include or are based on carbon nanotubes (CNTs) such as arrays, sheets, buckypapers, and yarns.<sup>[8–11]</sup> Although, these assemblies aim at exploiting the exceptional intrinsic properties, namely high electrical and thermal conductivity,<sup>[12,13]</sup> high strength and flexibility,<sup>[14]</sup> of an individual CNT at the macroscopic scale, they often show a remarkable drop (up to several orders of magnitude) of the abovementioned properties. This is related to the difficulty in achieving uniform distribution of catalysts, defect-free tubes, and an effective interfacial bonding between CNTs and the substrate.<sup>[9,10]</sup>


For example, the thermal conductivity of an individual multiwalled carbon nanotube (MWCNT) is several orders of magnitude higher than the effective one of a vertically aligned CNT (VA-CNT) foam-like nanostructure,  $136 \text{ W m}^{-1} \text{ K}^{-1}$  and  $1.04 \text{ W m}^{-1} \text{ K}^{-1}$ , respectively.<sup>[15]</sup> This decrease is mainly the result of the intertube scattering and the high thermal contact resistance at the CNT-substrate interface.

Interesting properties in nanoscale assemblies have been found by combining the high aspect ratio with thin conformal coatings. For example, photoanodes obtained by coating zinc oxide (ZnO) nanoforest with a thin layer of titanium dioxide ( $\text{TiO}_2$ ) for dye-sensitized solar cells,<sup>[16]</sup> or gold-coated vertical Si nanowires for biomolecule detection have been reported.<sup>[17]</sup>

In this perspective, VA-CNT arrays with their foam-like morphology represent an attractive 3D scaffold to create a novel class of high aspect ratio heterogeneous materials with tailored behavior. The tailoring of the CNT-based nanostructure performance strongly depends on the achieved porosity, the coating material and its infiltration within the nanotube network. Recently, Poelma et al. have shown how the mechanical response of high aspect ratio foam-like VA-CNTs can be tuned from foam-like toward brittle ceramic by simply varying the thickness of an amorphous silicon carbide coating.<sup>[18,19]</sup> No study has yet been published regarding the thermal conductivity enhancement consequent to the infiltration of a conformal coating within a porous VA-CNT array.

Dr. C. Silvestri, Dr. R. H. Poelma, A. Jovic, Dr. B. Morana, Dr. S. Vollebregt, Prof. G. Q. Zhang, Prof. P. M. Sarro  
Department of Microelectronics  
Delft University of Technology  
Feldmannweg 17, 2628CT Delft, The Netherlands  
E-mail: c.silvestri@tudelft.nl; P.M.Sarro@tudelft.nl

Dr. M. Riccio, Prof. A. Irace  
Department of Electrical Engineering and Information Technologies  
University of Naples Federico II  
Via Claudio 21, 80125 Naples, Italy

 The ORCID identification number(s) for the author(s) of this article can be found under <https://doi.org/10.1002/smll.201800614>.

DOI: 10.1002/smll.201800614

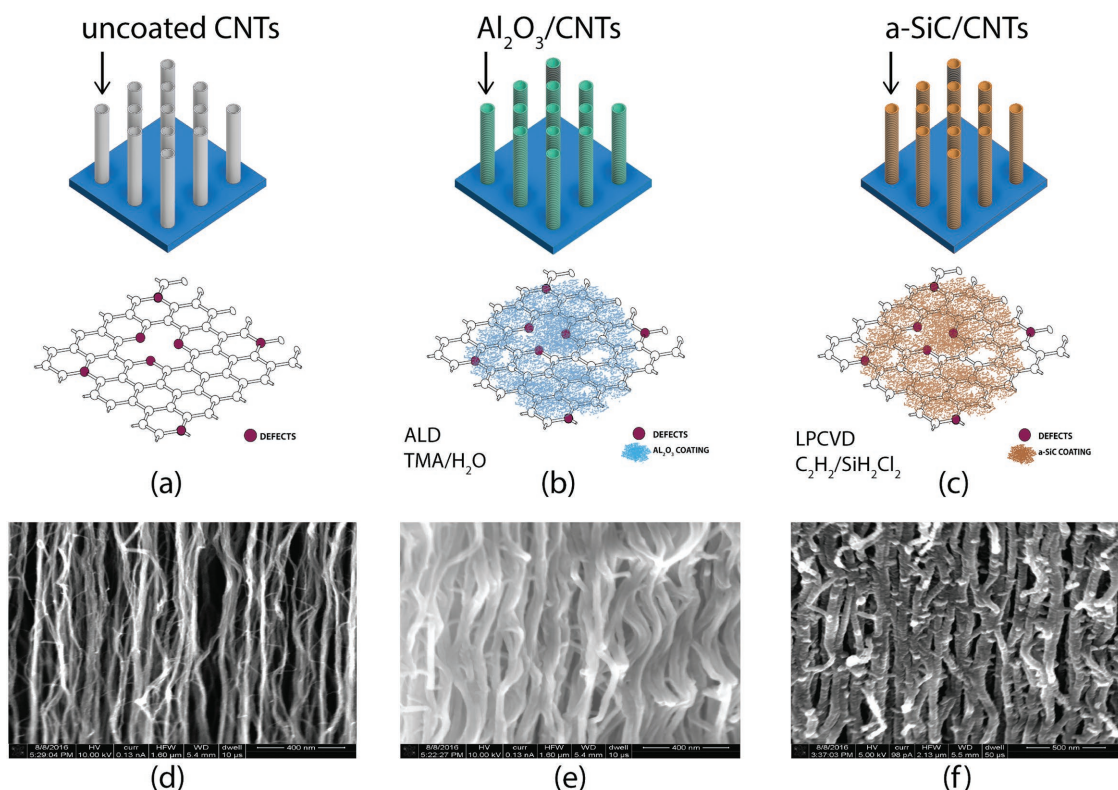


**Figure 1.** Coated  $\text{Al}_2\text{O}_3/\text{CNTs}$  and a-SiC/CNTs hybrid structures. The VA-CNTs are lithographically patterned to achieve micropin feature. a–c) Schematic illustration of 3D CNTs highlighting the gas precursors used during the coating procedure. d) SEM close-up of the as-grown VA-CNT array. The average nanotube diameter is 10 nm. e) SEM image of the obtained hybrid  $\text{Al}_2\text{O}_3/\text{CNTs}$  at the micropin sidewall. The resulting diameter of an individual nanotube is equal to 35 nm. f) SEM close-up of the a-SiC/CNT composite sidewall. The average diameter of an individual a-SiC coated CNT is 30 nm.

In this work, we explore the effect of nanoscale coatings on the thermal transport efficiency of high aspect ratio VA-CNTs expressed in terms of effective thermal conductivity,  $k_{\text{eff}}$ . The materials chosen to fill the VA-CNT-based scaffolds are aluminum oxide ( $\text{Al}_2\text{O}_3$ ) and nonstoichiometric amorphous silicon carbide (a-SiC). They are both ceramic-like materials with superior hardness, and large thermal conductivity,  $\approx 360 \text{ W m}^{-1} \text{ K}^{-1}$  and  $\approx 25 \text{ W m}^{-1} \text{ K}^{-1}$  for bulk SiC and bulk  $\text{Al}_2\text{O}_3$ , respectively.<sup>[20,21]</sup> We begin by locally synthesizing various VA-CNT micropin configurations on top of microelectromechanical systems (MEMS) microhotplates (MHP), used both as heat source and thermal sensor. For further details on the fabrication process of the MHP and CNT synthesis, we refer to our previous publication.<sup>[15]</sup> After the growth step, the VA-CNTs are coated by using atomic layer deposition (ALD) for the  $\text{Al}_2\text{O}_3$  and by low-pressure chemical vapor deposition (LPCVD) for the a-SiC, to achieve a targeted coating thickness of 15 nm. The chosen deposition techniques allow to obtain nanoscale accuracy over the deposition thickness and a good conformality. The formation of the heterogeneous composites, the  $\text{Al}_2\text{O}_3$  coated ( $\text{Al}_2\text{O}_3/\text{CNTs}$ ) and the a-SiC coated (a-SiC/CNTs) CNT nanofoam scaffolds, is sketched in **Figure 1a–c**. It is well known that CVD-grown CNTs have a high density of surface defects in comparison to CNTs fabricated by arch-discharge or laser ablation methods. This represents an advantage as the surface defects provide bonding sites for the coating nucleation.<sup>[22,23]</sup> As shown by the Raman spectra of the

as-grown CNTs (Figure S1, Supporting Information), the intensity ratio between the D- and G-band peaks ( $I_D/I_G$ ) is equal to 0.95, revealing the low crystallinity degree of the CNT sample. Therefore, due to their intrinsic defectivity, no functionalization treatments are performed on the CNT scaffold prior to the coating procedures. Upon exposure to the precursor gases, the corresponding precursor molecules diffuse into the VA-CNT porous structure. The coating nucleation starts from the interaction between precursor gases and localized CNT surface defect sites, and/or precursors and CNT–CNT junctions. The product of the reaction is a nanometer-size granule formation at the surface. A thin layer is then formed by the overlap of adjacent grains while the number of cycles or the deposition time increases, depending on the adopted deposition technique (ALD or LPCVD).

Scanning electron microscope (SEM) images of VA-CNT sidewalls reported in **Figure 1d–f**, highlight the morphological variation of the cluster surface before and after the coating depositions. The as-grown VA-CNT array consists of wavy interlaced multiwalled carbon nanotubes, oriented perpendicular to the substrate. The bridging between nearby nanotubes creates a regular foam-like structure with an average spacing of 60 nm.

The nanotube average diameter,  $d_{\text{CNT}}$ , is 10 nm and the tube density within the micropin is around  $112 \text{ tubes } \mu\text{m}^{-2}$ , resulting in a porosity of 99.1% (**Figure 1d**). For ideally aligned CNTs a 30 nm coating can not only fill but also coalesce the entire array.

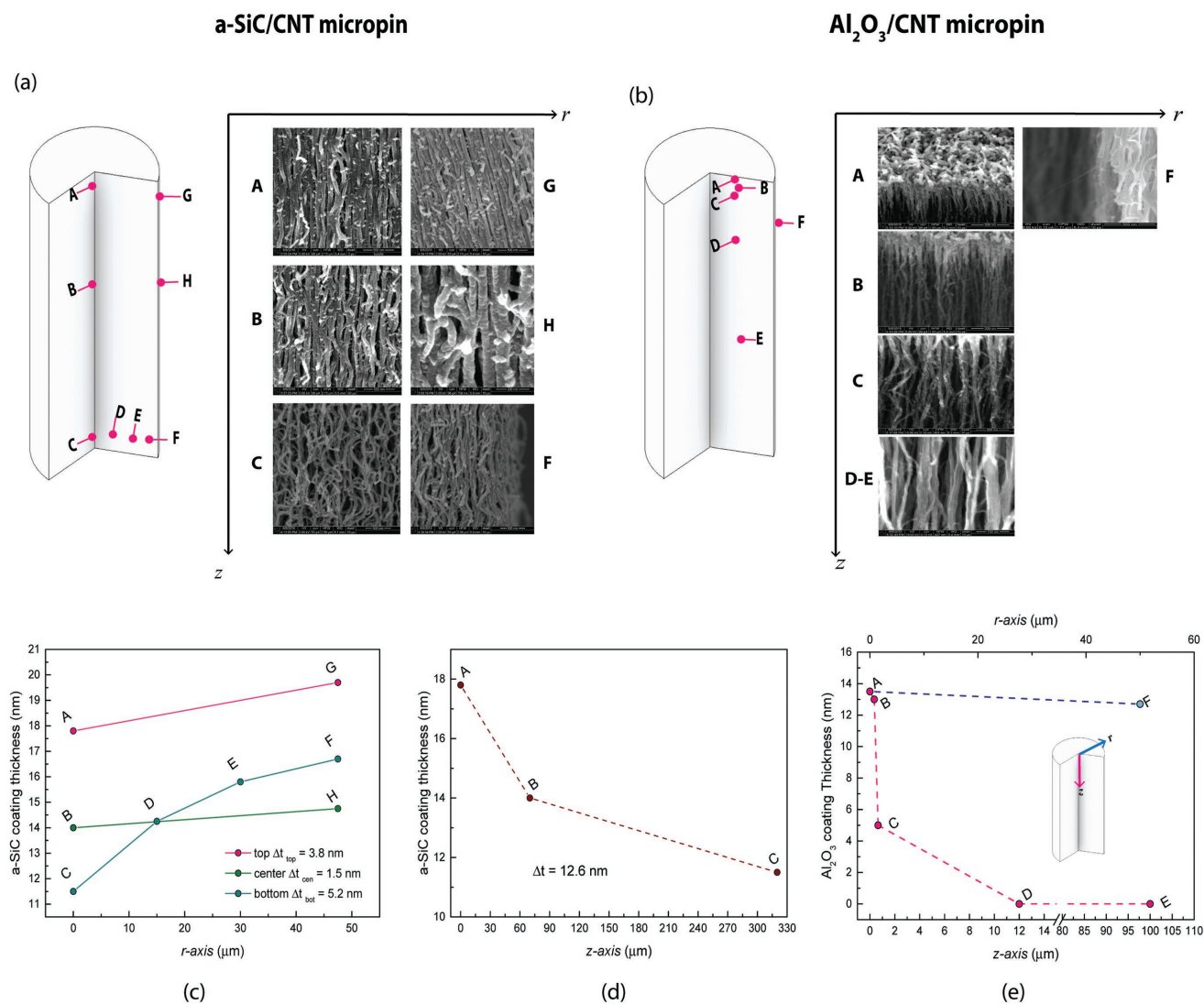


**Figure 2.** a) Penetration depth of the LPCVD a-SiC coating in the CNT micropin. On the 3D micropin illustration the location of the points analyzed by SEM is reported. b) The penetration depth of the ALD Al<sub>2</sub>O<sub>3</sub> coating in the CNT micropin. On the 3D micropin illustration the location of the points analyzed by SEM is reported. c,d) The graphs report the thickness variation along the z- and r-directions of the a-SiC/CNT micropin. e) The graph reports the thickness variation along z- and r-directions of the Al<sub>2</sub>O<sub>3</sub>/CNT micropin.

Both micropin hybrid composites studied show remarkably uniform deposition around the nanotubes. The initial vertical orientation and the high surface area of the CNT array are retained, while in correspondence to the CNT–CNT junctions some localized aggregations are formed. The average CNT coated diameter is 31 and 35 nm for the Al<sub>2</sub>O<sub>3</sub>/CNTs and for the a-SiC/CNTs, respectively (Figure 1e,f). Therefore, the average coating thicknesses deposited on the MWCNT surface are ≈17 nm for the a-SiC and ≈13 nm for the Al<sub>2</sub>O<sub>3</sub>, in good agreement with the ones measured by ellipsometry on a bare silicon wafer.

In order to investigate the morphology and the coating infiltration depth within the VA-CNT arrays, we performed high-resolution SEM pictures at different microstructure locations, from top to bottom of the micropin (z-axis) as well as along the radius (r-axis). The coating uniformity and the penetration

depth of both the a-SiC/CNTs and the Al<sub>2</sub>O<sub>3</sub>/CNTs are reported in Figure 2.

The a-SiC coated micropin (Figure 2c) shows an excellent coating penetration along the radial direction. In particular, for every 1 μm, the coating reduces of roughly 0.1 nm when going from the sidewall to the core. The thickness variation along the z-axis is just 6 nm over the full micropin height (Figure 2d). The remarkable coating infiltration of LPCVD a-SiC was also observed in other works focused on others materials.<sup>[24–27]</sup>

From the analysis of the Al<sub>2</sub>O<sub>3</sub> coated micropin, the coating at the sidewall looks uniform. However, after cleavage, the SEM analysis of the micropin cross-section reveals a poor and uneven infiltration of the precursors through the CNT array (Figure 2b), demonstrating a diffusion-limited mechanism for the coating. The achieved heterogeneous material is made of a soft core of uncoated CNTs reinforced by a ceramic shell, which

is  $\approx 1.4 \mu\text{m}$  thick, as shown Figure S3 (Supporting Information). The coating thickness along the  $z$ -axis is  $\approx 13.5 \text{ nm}$  at the micropin tip ( $z = 0$ ), it reduces down to  $5 \text{ nm}$  at  $z = 650 \text{ nm}$  (Figure 2e). For  $z > 650 \text{ nm}$  some isolated grains can be noted, while the coating traces disappear completely for  $z > 12 \mu\text{m}$ . The same abrupt reduction in the coating thickness occurs along the  $r$ -axis (Figure 2e). The coating thickness reduces  $\approx 12.8 \text{ nm}$  every  $1 \mu\text{m}$ .

The resulting coating penetration depths are  $\approx 700 \text{ nm}$  for the ALD coated  $\text{Al}_2\text{O}_3/\text{CNTs}$  and around  $66 \mu\text{m}$  for the LPCVD a-SiC/CNTs, proving the superior ability of the LPCVD process to evenly coat complex high surface area nanostructures. The low penetration depth and the uneven uniformity of the ALD coating within the intricate CNT foam-like morphology has been the object of several studies.<sup>[23,28,29]</sup> The relatively low temperature of the ALD process represents the main limiting factor of the coating process itself. The initial diffusion of precursor molecules inside the foam is slow and it decreases with increasing the individual CNT diameters. After each cycle, the CNT–CNT spacing reduces while the CNT surface area increases, limiting the diffusion coefficient even further. To achieve a uniform monolayer on a large surface area as the one of the VA-CNT array, a cycle-to-cycle variation in both precursor dose and purging time are required.<sup>[28,30,31]</sup>

As mentioned before, the aim of this work is to explore the effect of nanoscale coating on the thermal transport properties of coated VA-CNTs. The adopted measurement approach consists of an MHP on which two different VA-CNT configurations have been directly synthesized: a multipin configuration, composed by six micropins (each with a radius of  $10 \mu\text{m}$ ), and a single micropin ( $100 \mu\text{m}$  in radius), shown in the insets of Figure 3.

**Thermal Performance of a-SiC/CNT Multipin:** The VA-CNT multipin arrangement shows remarkable enhancement of the heat dissipation performance after the a-SiC coating (Figure 3a). To understand which of the heat transfer mechanisms can be the cause of such improvement, we characterized the samples in two different environmental conditions: in vacuum and in air.

In vacuum, the heat conducted through the VA-CNTs is dissipated by radiation. The evaluation of the emissivity ( $\epsilon$ ) by high-resolution infrared microscopy reveals an unvaried  $\epsilon$  between the coated and uncoated VA-CNTs ( $\epsilon = 0.95$ ). Moreover, the overall shape of the multipin configuration is substantially unaltered due to the nanometer-thick coating. Therefore, the substantial improvement obtained in vacuum is due to an enhanced effective thermal conductivity,  $k_{\text{eff a-SiC/CNT}}$ . Secondary effects, such as annealing and influence of the a-SiC coating on the MHP, can be excluded. First, the Pt spiral on which the MHP is based was preannealed at  $1000 \text{ }^\circ\text{C}$  for one hour during the fabrication process. Second, a bare reference MHP without CNT underwent the same coating as the VA-CNT samples and any variation in thermal performance prior and after the coating procedure was detected.

In air, the difference between the pre- and postcoating heat dissipative behaviors is even more remarkable. For example, for a given input power of  $25 \text{ mW}$  a reduction of the local hot-spot temperature of  $103 \text{ K}$  is achieved in air. The heat dissipation improvement recorded in air is related to both conduction and

convection, and therefore it can be related to the  $k_{\text{eff a-SiC/CNT}}$  and to the porosity variation. The specific impact of each of the above-mentioned contributions needs to be determined.

**Thermal Performance of a-SiC/CNT Single Micropin:** Unexpectedly, the a-SiC/CNT single micropin does not show a detectable heat transfer improvement before and after the coating (Figure 3b). The extraordinary performance improvement of the multipin configuration (up to 75% more power dissipated in air and 64% in vacuum) and the unvaried performance of the single micropin poses many questions. The unvaried single micropin behavior may be partially related to the micropin's geometry and diameter. As previously mentioned, the maximum micropin radius to achieve evenly coated a-SiC/CNTs is  $66 \mu\text{m}$ . Consequently, the entire volume of each multipin element ( $10 \mu\text{m}$  in radius) is fully coated, while the single micropin volume that is effectively coated is about 88% of the total.

**Thermal Performance of  $\text{Al}_2\text{O}_3/\text{CNT}$  Configurations:** No evidence of heat dissipation enhancement is found for any investigated CNT configuration after the ALD  $\text{Al}_2\text{O}_3$  coating treatment (Figure 3c,d). This is explained by the observed low infiltration depth of the coating within the VA-CNTs.

To highlight how the two coatings affect the heat dissipation, we report in Figure 3e,f the average temperature reached by the various arrangements at a fixed power. In both air and vacuum, the a-SiC coated multipin configuration,  $T_{\text{6ma-SiC}}$ , outperforms the others. The unaltered heat transfer performances of the  $\text{Al}_2\text{O}_3/\text{CNTs}$  and the impressive enhancement of the a-SiC multipin scaffolds might be related to the effective thermal conductivity and the porosity variation. In the following, these two main causes are discussed.

**Effective Thermal Conductivity:** The effective thermal conductivity data are obtained by relating the temperature at the micropin tip and at the junction region CNTs-MHP, measured by high-resolution IR microscopy, with the 1D pin fin heat transfer model explained in a previous publication.<sup>[15]</sup> The temperature dependency of the  $k_{\text{eff}}$  of both  $\text{Al}_2\text{O}_3$  and a-SiC VA-CNT multipins is obtained by acquiring the IR maps while powering the MHP (Figure 4a,b).

Figure 4c shows the obtained  $k_{\text{eff}}$  of the pre- (named  $k_{\text{eff CNT}}$ ) and postcoated multipin arrangements (named  $k_{\text{eff a-SiC/CNT}}$  and  $k_{\text{eff Al}_2\text{O}_3/\text{CNT}}$ ) at different temperatures. The  $k_{\text{eff Al}_2\text{O}_3/\text{CNT}}$  shows no substantial variation compared to the uncoated VA-CNTs, in line with the power dissipation recorded. For the a-SiC/CNTs instead, the graph clearly reveals a strong  $k_{\text{eff}}$  enhancement due to the conformal coating penetration into the CNT nanofoam architecture. At the lowest investigated temperature, the  $k_{\text{eff}}$  improved from  $1.04 \text{ W m}^{-1} \text{ K}^{-1}$ , when uncoated, to  $2.6 \text{ W m}^{-1} \text{ K}^{-1}$  when a-SiC coated. The  $k_{\text{eff a-SiC/CNT}}$  reaches  $4.2 \text{ W m}^{-1} \text{ K}^{-1}$  at the highest investigated temperature. In particular, the  $k_{\text{eff a-SiC/CNT}}$  trend shows a steep increase around  $392 \text{ K}$ , while for higher temperature the increase rate reduces. The enhancement factor,  $\eta$ , defined by the ratio

$$\eta = \frac{k_{\text{eff a-SiC/CNT}} - k_{\text{eff CNT}}}{k_{\text{eff CNT}}} \quad (1)$$

highlights the conductive transport enhancement at different operating temperatures and it goes from 104% up to 181%

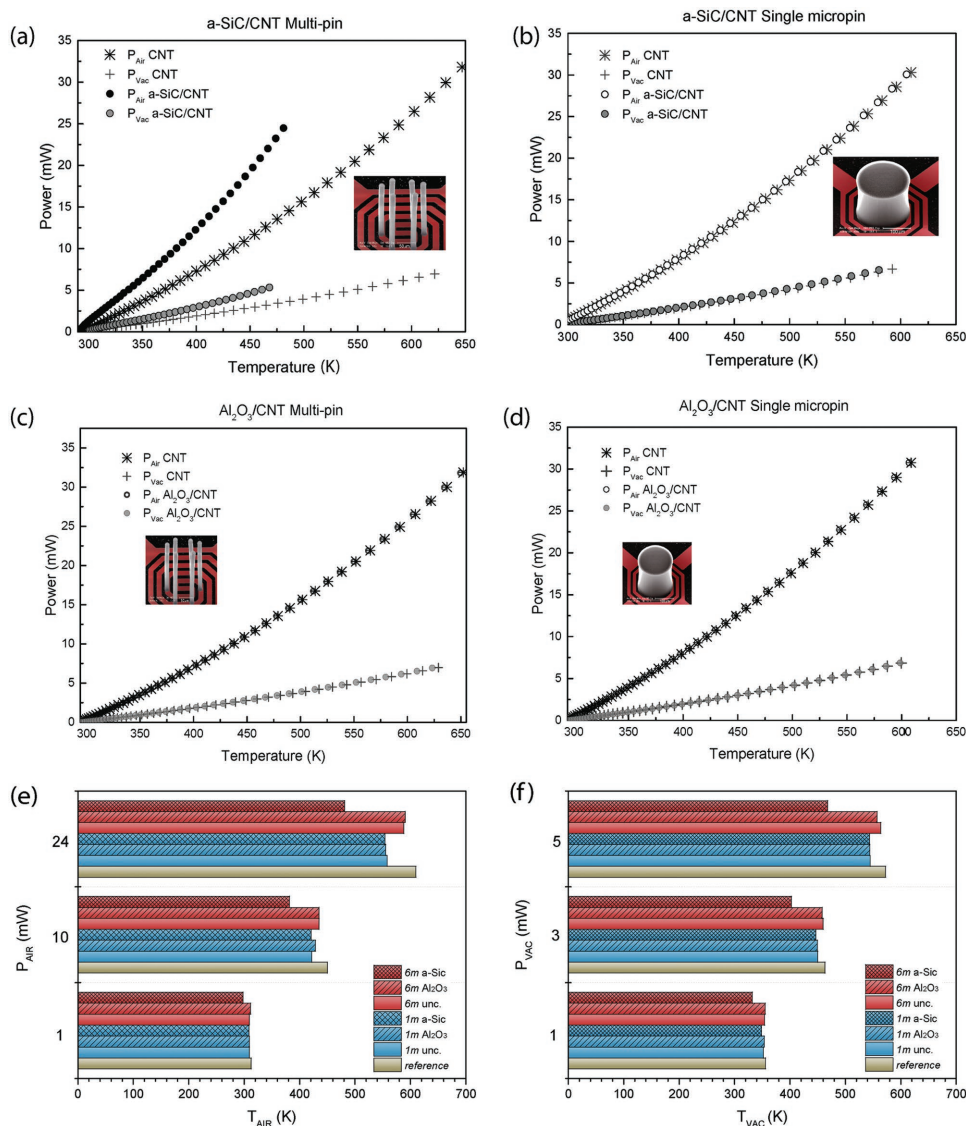


**Figure 3.** Power versus temperature trend before and after a,b) the a-SiC and c,d)  $\text{Al}_2\text{O}_3$  coatings (CNT, a-SiC/CNT, and  $\text{Al}_2\text{O}_3$ /CNT in the legend) for two sample configurations: a,c) the multipin and b,d) the single micropin. The measurements were performed in air and vacuum ( $P_{\text{AIR}}$  and  $P_{\text{VAC}}$ ). The “\*” and “+” symbols refer to  $P_{\text{AIR}}$  and  $P_{\text{VAC}}$  of the uncoated configurations, respectively, while “•” refers to the same sample after the nanoscale coatings. e,f) Average temperature ( $T_{\text{AIR}}$  or  $T_{\text{VAC}}$ ) reached by the analyzed sample sets for a given input power in e) air,  $P_{\text{AIR}}$ , and in f) vacuum,  $P_{\text{VAC}}$ . The 6 m, 1 m, and reference labels refer to the multipin, single micropin, and bare MHP, respectively. The unpatterned bars indicate the samples taken as reference (uncoated VA-CNTs or bare MHP).

(Figure 4b). The obtained results draw further attention to the impressive effect that the amorphous carbide coating has on the improvement of thermal performance efficiency of VA-CNT scaffolds. To the best of our knowledge, this is the highest-ever reported thermal conductivity enhancement of VA-CNTs obtained by nanolayer coating.

It is generally recognized that thermal conduction in CNT arrays strongly depends on their morphology, vacancies, defects and CNT–CNT interactions as well as the thermal boundary resistance at the CNT-substrate and CNT-air interfaces. As shown by the SEM picture (Figure S2, Supporting Information) and by the  $I_D/I_G$  ratio, the as-grown foam-like morphology consists of many defects, CNT–CNT junctions, and twists that highly affect the thermal transport and increase the

phonon-boundary scattering. It has been demonstrated that the thermal resistance at the interface between two nanotubes, which interact through van der Waals forces, is notably large (tube–tube thermal resistance  $\approx 11 \times 10^{-8} \text{ m}^2 \text{ K W}^{-1}$ ).<sup>[32,33]</sup> All these aspects are reflected in the achieved  $k_{\text{eff CNT}}$ . The factors that might explain the thermal conductivity enhancement of the a-SiC/CNT composite are the nanocoating conformality, the intrinsic thermal conductivity of the deposited material, which can be higher than MWCNTs, and a reduction in the CNT-substrate contact resistance.

By conformally coating a VA-CNT scaffold a new percolating network is built on top of the original one, allowing to overcome defected regions, tube twists, and to promote additional heat conduction paths, thus enhancing the phonon transfer

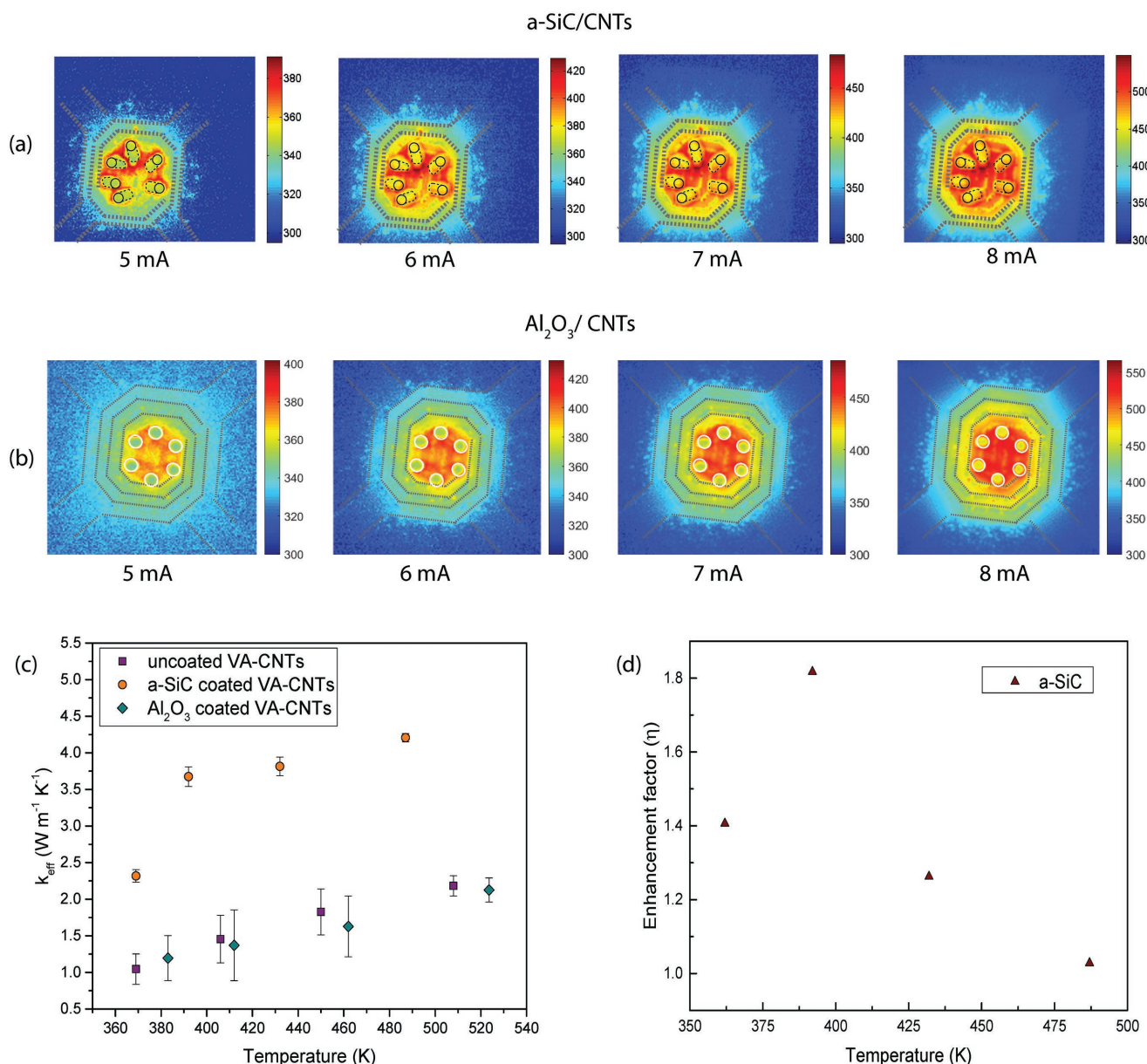


**Figure 4.** High-resolution IR maps of the multipin configuration of a) a-SiC/CNTs and b) Al<sub>2</sub>O<sub>3</sub>/CNTs at four current inputs: 5, 6, 7 and 8 mA. The MHP structure is highlighted by the gray line. c) Temperature dependence of the experimentally determined  $k_{\text{eff}}$  for uncoated (purple), a-SiC coated (orange) and Al<sub>2</sub>O<sub>3</sub> coated (dark cyan) VA-CNTs. d) The thermal conductivity enhancement,  $\eta$ , is reported as a function of temperature. The a-SiC coated sample reaches an enhancement up to 181%.

among contiguous CNTs.<sup>[34]</sup> In fact, the CNT–CNT contact area increases while the interfacial thermal resistance between neighboring CNTs is reduced.<sup>[33]</sup> Moreover, new contact points are created, which may lead to an increase in phonon scattering phenomena as well as to additional paths for heat transfer among adjacent tubes that were not in contact before.<sup>[35]</sup> The Al<sub>2</sub>O<sub>3</sub> coating, with its inability to create a conductive network spread over the whole scaffold surface and its scarce penetration depth, prevents any significant heat transfer improvement (Figure 4c).

Another possible enhancement factor is the thermal conductivity of the a-SiC itself. Since the coating thickness is close

to the phonon mean free path of both the MWCNTs (as low as 4 nm)<sup>[36]</sup> and the a-SiC (as low as 0.488 nm),<sup>[37]</sup> the thermal conductivity ceases to be a material property and becomes dependent on size and shape of the boundary interface.<sup>[38]</sup> It has been reported that for thin films the thermal conductivity of amorphous SiC is likely to be rather smaller than for the bulk crystalline structure, 0.12–3.6 W m<sup>-1</sup> K<sup>-1</sup> instead of 320–490 W m<sup>-1</sup> K<sup>-1</sup>.<sup>[37]</sup> However, it is higher than  $k_{\text{eff,CNT}}$ .

Last but not least,  $k_{\text{eff,CNT}}$  can increase due to a reduction of the thermal contact resistance at the CNT–substrate interface. It has been demonstrated that in presence of a weak bond between the substrate and the nanofoam, not all the CNTs



participate effectively in the heat transport.<sup>[39]</sup> A better thermal coupling between the support layer and the CNTs can be achieved through embedding the nanotube in a metal contact or increasing the contact area by pressing the CNTs toward the substrate.<sup>[40,41]</sup> In our case, by performing the coating it might likely be that more CNTs are participating to the heat transfer due to the cross-sectional area enhancement given by the a-SiC coating.

*Porosity:* Another possible reason for the recorded impressive enhancement of the thermal performance of the a-SiC coated multipin configuration can be related to the porosity variation. The foam-like VA-CNT porosity of a multipin element reduces from 99.1% to 85.5% in consequence of the a-SiC coating infiltration. Based on the micropin model described in the Supporting Information (Equation S1), we calculate the heat loss through a unit element and the whole multipin configuration,  $Q_{\text{pin}}$  and  $Q_{\text{Tipin}}$ , respectively. The discrepancy between the measured heat transfer rate ( $Q_{\text{Tipin}}^*$ ) and the theoretical heat transfer rate ( $Q_{\text{Tipin}}$ ) is about 2% for the uncoated VA-CNT configuration, while it is about 62% for the a-SiC coated one (see Table S1 in the Supporting Information). The substantial discrepancy observed in the a-SiC/CNTs multipin configuration is most likely caused by the porosity variation, which is not included in the adopted model.

The porosity reduction, consequent to the nanoscale conformal coating, affects the natural convective heat flow as well as the heat transfer. The natural convective heat flow is influenced by two opposite factors. It should decrease due to less air passing through the pores created by the VA-CNT matrix, because the volume filling fraction of CNTs increases, while the air volume and the flow within the micropin decreases. At the same time, the heat convection should increase due to the increase in the effective surface area of the micropin after coating, which implies that more heat is convected to the surrounding. To quantify how these factors can mutually compensate each other at the nanometer scale is hard and requires an in-depth investigation. However, the enhanced heat transfer rate after a-SiC coating suggests that the surface-to-volume ratio increase has a stronger influence than the internal air volume reduction.

In addition to the thermal performance enhancement, the infiltration of the a-SiC conformal coating into foam-like VA-CNTs enforces the mechanical stability of the achieved micropins, as evidenced by their successful encapsulation in an epoxy molding compound (described below).

*Through-Package Thermal Vias Based on a-SiC VA-CNTs:* Here for the first time, we report on through-package thermal vias based on VA-CNT micropins. They can represent an attractive alternative as thermal as well as electrical vias. The bottom-up growth, the possibility to fully customize both feature shape and aspect ratio, and the chance to tailor their mechanical, thermal and electrical behavior through conformal coatings make VA-CNT arrays a promising candidate as CNT-based vias. A preliminary study is carried out to prove the possibility to embed a-SiC coated VA-CNT micropins into a wafer-level packaging process. Patterned VA-CNT arrays are grown on a Si wafer reaching a height of around 300  $\mu\text{m}$ . After conformally coating the nanotubes with 20 nm of LPCVD a-SiC, a film-assisted molding (FAM) conducted at wafer-scale to encapsulate the system is performed. The FAM is a proprietary technology of Boschman Technologies

and the Advanced Package Center.<sup>[42]</sup> The crucial part of the encapsulation process is that VA-CNT micropins must withstand the pressure (from 3 to 80 bar) used to insert the epoxy molding compound, therefore proper anchoring with the substrate and good mechanical strength are necessary. After the encapsulation, the wafer is diced into individual chips of  $6 \times 6 \text{ mm}^2$ . Figure 5a–f shows micropins with different diameters before and after the coating and the resulting VA-CNT vias through the epoxy molding compound (Figure 5g–i). The molding is quite uniform over the entire wafer and most of the VA-CNT micropins have the tip sticking out from the molding, allowing to perform subsequent optional metallization for routings useful in, e.g., electrical vias. Figure S4 (Supporting Information) shows the compressive failure of some micropins, probably occurred during the closure and clamping of the top mold. The compressive failure mechanism observed in our 15 nm coated a-SiC micropins has been extensively studied by others.<sup>[18,19]</sup>

The obtained chip-interposer has been thermally characterized by high-resolution IR microscopy. The interposer is heated up via a thermal chuck to temperatures ranging from 180 °C to 210 °C. By focusing on the chip area, the surface temperature reached by the interposer is monitored. The collected data are then compiled into thermal maps (Figure S5, Supporting Information). Each map clearly shows the VA-CNT micropin tip temperature, which is lower than the temperature of the heated chuck, and the symmetric temperature profile along their radius, confirming the conformality of the a-SiC scaffold for different micropins diameters.

However, to avoid possible artifacts in recording the surface temperature, due to the low distance (4 to 5 cm) between the heated chuck and the optics used to record the IR emission, a higher working distance is required. Therefore, with the current device configuration it is not possible to estimate the heat loss through the VA-CNT vias and the epoxy molding compound. Further tests need to be carried out.

This work discussed the effects of ceramic coatings on the thermal performance of high aspect ratio VA-CNT micropins. VA-CNT configurations directly grown on top of MHPs are subjected to a coating process with ALD  $\text{Al}_2\text{O}_3$  and LPCVD a-SiC as coating materials. The thermal response of micropin configurations is characterized prior and after depositing the coatings, using a combination of Joule heating and IR microthermography. The obtained  $\text{Al}_2\text{O}_3$ /CNT hybrid material shows no significant variation in terms of heat dissipation compared to the uncoated one. We conclude that the unvaried behavior is caused by the limited penetration depth of the ALD precursors within the CNT nanofoam. The a-SiC/CNT instead shows a tremendous increase of the effective thermal conductivity by 181% compared to the as-grown CNT nanofoam. According to the obtained results and the morphological analysis, the key factor for CNT thermal transport enhancement is the precursor penetration within the nanofoam morphology. In fact, the sole presence of a thin shell of coating around the micropin does not improve the overall performance. It is the formation of a 3D network across the entire micropin that contributes to the great enhancement of the thermal conductivity, by reducing the interfacial thermal resistance between tubes and between CNTs and the substrate and by providing additional thermal paths for the heat carriers.

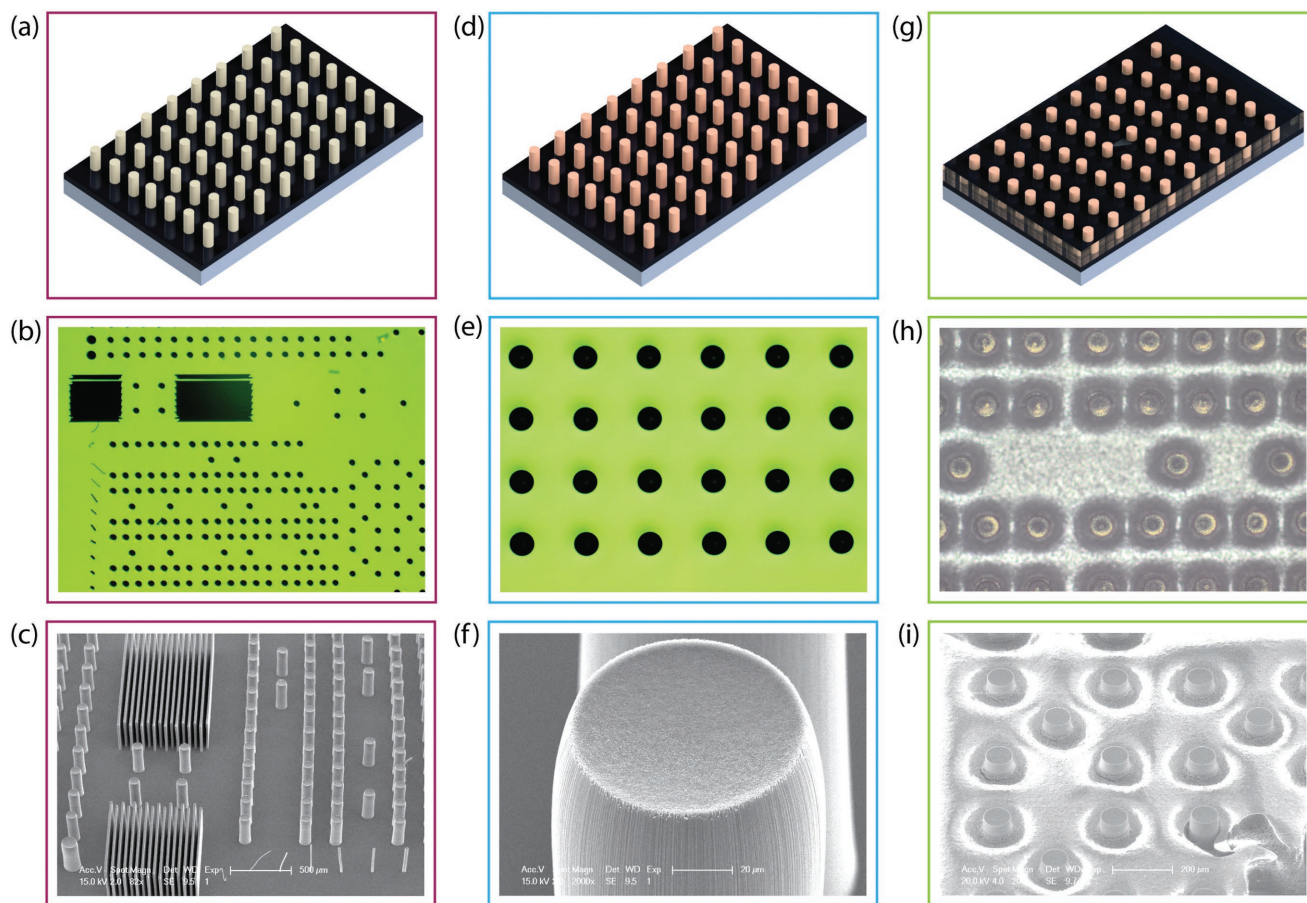


**Figure 5.** a) Photo-lithographically patterned VA-CNT micropins are grown on a Si/SiO<sub>2</sub>/Al<sub>2</sub>O<sub>3</sub> stack. b,c) Optical and SEM images of the as-grown VA-CNT micropins, with diameters ranging from 10 to 100 μm and height of 300 μm. d–f) A 15 nm coating of a-SiC infiltrates the VA-CNTs. g) A layer of epoxy molding compound is inserted. h,i) Optical and SEM images showing, for the first time, the micropins enclosed into the molding by FAM.

Natural convective heat-transfer in porous media is an active research area field.<sup>[43–45]</sup> To fully understand the natural convective heat-transfer in foam-like VA-CNTs, including porosity variations, in-depth numerical modeling and experimental studies are needed.

The achieved heterogeneous material can be interesting for a wide range of applications spanning from solid-state supercapacitors,<sup>[30]</sup> to through-silicon-via interconnects,<sup>[11]</sup> to on-chip cooling solutions.<sup>[15]</sup> In particular, to prove that high aspect ratio conformally coated VA-CNTs can be used as 3D microstructure for localized and customized microcooling solutions, a chip-interposer is fabricated by wafer-scale FAM. The encapsulation was successful due to the increased mechanical stability provided by the a-SiC conformal coating. A future step will be to understand the heat transfer of the interposer-chip, by obtaining more reliable IR maps and by using it as interposer among chip stacks. This work highlights the opportunities provided by applying conformal coatings on VA-CNTs.

## Experimental Section

**Synthesis of VA-CNT:** Vertically aligned CNTs were synthesized at wafer-scale on a 30 nm sputtered Al<sub>2</sub>O<sub>3</sub> barrier layer on which 1.2 nm

of iron (Fe) catalyst nanoparticles was evaporated and patterned by lift-off to define the micropin geometry. The substrate on which VA-CNTs were synthesized consisted of Pt microheaters (90 in total) embedded on a 400 nm silicon nitride membrane supported by a 4" silicon wafer. Further details on the fabrication process of the MHPs and the CNT synthesis can be found elsewhere.<sup>[17,46]</sup> The wafer was then loaded in a commercial chemical vapor deposition (CVD) system at 650 °C for 5 min using H<sub>2</sub>/C<sub>2</sub>H<sub>2</sub> as feedstock at a pressure of 80 mbar.

**Coating Procedure:** To perform the a-SiC conformal coating, the samples were loaded into a Tempress hot-wall LPCVD furnace. The precursor gasses were acetylene (C<sub>2</sub>H<sub>2</sub>) and dichlorosilane (SiH<sub>2</sub>Cl<sub>2</sub>) diluted in 5% hydrogen (H<sub>2</sub>) and the deposition temperature and pressure were fixed at 760 °C and 0.8 mbar, respectively. Most probably the coating nucleation started from CNT surface defects. The average a-SiC deposition rate was 5 Å min<sup>-1</sup>, with an incubation time of ≈7 min before the film growth starts. A detailed description of the physical and chemical properties of the deposited a-SiC thin layer can be found in ref. [47].

The Al<sub>2</sub>O<sub>3</sub> conformal coating was applied using an ALD system (ASM F-120). The deposition temperature was set at 300 °C and the pressure at 1.33 mbar. The ALD cycle sequence consisted on exposing the sample to trimethylaluminum for 2 s, then to a nitrogen (N<sub>2</sub>) purge for 6 s, followed by 2 s of high purity water (H<sub>2</sub>O) exposure, ending with 8 s of N<sub>2</sub> purge. The N<sub>2</sub> purge was performed after each precursor exposure to remove any unreacted precursors or reaction by-products from the chamber. The average deposition rate was self-limited to around 0.9 nm per cycle.

**Thermal Performance Characterization:** To quantify the heat dissipation through the investigated micropin configuration MHPs on which VA-CNTs are directly synthesized were used. The MHP was designed to generate heat by Joule heating as well as to sense the average device temperature. The characterization was performed by loading the MHP in a stainless still vacuum chamber, equipped with four probe needles, connected to a vacuum pump and a probe station. The setup allowed performing measurements under two environmental conditions: vacuum and ambient pressure.

**Thermal Conductivity Characterization:** To quantify the  $k_{\text{eff}}$  of coated and uncoated multipin configurations, a combination of electrical stimulation and high-resolution thermographic microscopy analysis (temperature sensitivity of 1 K and spatial resolution of 2.5  $\mu\text{m}$ ) was used. Prior to recording the temperature of the VA-CNTs under tests, a calibration procedure of the state-of-the-art IR system was performed, based on the two-point algorithm.<sup>[48]</sup> The temperature distribution of the coated and uncoated multipin configurations was recorded for four power values by Joule-heating the device with a stepwise current from 5 to 8 mA.

## Supporting Information

Supporting Information is available from the Wiley Online Library or from the author.

## Acknowledgements

This work was supported by NanoNextNL, a micro and nanotechnology consortium of the Government of the Netherlands and 130 partners. The authors gratefully acknowledge the technical staff of the Else Kooi Laboratory (former DIMES Technology Center) at TU Delft for the support in device fabrication. The authors thankfully acknowledge the equipment resources, technical expertise and assistance provided by Boschman Technologies and the Advanced Package Center.

## Conflict of Interest

The authors declare no conflict of interest.

## Keywords

carbon nanotubes, conformal coating, epoxy molding, thermal property, vertically aligned

Received: February 9, 2018

Revised: March 5, 2018

Published online: April 17, 2018

- [1] B. I. Kharisov, O. V. Kharissova, B. O. García, Y. P. Méndez, I. G. de la Fuente, *RSC Adv.* **2015**, *5*, 105507.
- [2] S. Vollebregt, F. D. Tichelaar, H. Schellevis, C. I. M. Beenakker, R. Ishihara, *Carbon* **2014**, *71*, 249.
- [3] S. K. Balasingam, M. G. Kang, Y. Jun, *Chem. Commun.* **2013**, *49*, 11457.
- [4] J. A. Fairfield, *Adv. Funct. Mater.* **2017**, 1701145, <https://doi.org/10.1002/adfm.201701145>.
- [5] J. Rivnay, H. Wang, L. Fenno, K. Deisseroth, G. G. Malliaras, *Sci. Adv.* **2017**, *3*, e1601649.
- [6] L. Huang, Q. Wei, R. Sun, L. Mai, *Front. Energy Res.* **2014**, *2*, 43.

- [7] D. P. Dubal, D. Aradilla, G. Bidan, P. Gentile, T. J. S. Schubert, J. Wimberg, S. Sadki, P. Gomez-Romero, *Sci. Rep.* **2015**, *5*, 9771.
- [8] M. D. Lima, N. Li, M. Jung de Andrade, S. Fang, J. Oh, G. M. Spinks, M. E. Kozlov, C. S. Haines, D. Suh, J. Foroughi, S. J. Kim, Y. Chen, T. Ware, M. K. Shin, L. D. Machado, A. F. Fonseca, J. D. W. Madden, W. E. Voit, D. S. Galvão, R. H. Baughman, *Science* **2012**, *338*, 928.
- [9] A. E. Aliev, M. H. Lima, E. M. Silverman, R. H. Baughman, *Nanotechnology* **2010**, *21*, 035709.
- [10] M. B. Jakubinek, B. Ashrafi, J. Guan, M. B. Johnson, M. A. White, B. Simard, *RSC Adv.* **2014**, *4*, 57564.
- [11] S. Vollebregt, S. Banerjee, F. D. Tichelaar, R. Ishihara, *Microelectron. Eng.* **2016**, *156*, 126.
- [12] P. Kim, L. Shi, a. Majumdar, P. L. McEuen, *Phys. Rev. Lett.* **2001**, *87*, 215502.
- [13] T. W. Ebbesen, H. J. Lezec, H. Hiura, J. W. Bennett, H. F. Ghaemi, T. Thio, *Nature* **1996**, *382*, 54.
- [14] B. Demczyk, Y. Wang, J. Cummings, M. Hetman, W. Han, A. Zettl, R. Ritchie, *Mater. Sci. Eng., A* **2002**, *334*, 173.
- [15] C. Silvestri, M. Riccio, R. H. Poelma, B. Morana, S. Vollebregt, F. Santagata, A. Irace, G. Q. Zhang, P. M. Sarro, *Nanoscale* **2016**, *8*, 8266.
- [16] C. M. Lin, Y. C. Chang, J. Yao, C. Wang, C. Luo, S. (Shizhuo) Yin, *Mater. Chem. Phys.* **2012**, *135*, 723.
- [17] I. Kim, S. E. Kim, S. Han, H. Kim, J. Lee, D.-W. Jeong, J. J. Kim, Y. B. Lim, H. J. Choi, *Nanoscale Res. Lett.* **2013**, *8*, 502.
- [18] R. H. Poelma, B. Morana, S. Vollebregt, E. Schlangen, H. W. van Zeijl, X. Fan, G. Q. Zhang, *Adv. Funct. Mater.* **2014**, *24*, 5737.
- [19] R. H. Poelma, X. Fan, Z. Y. Hu, G. Van Tendeloo, H. W. van Zeijl, G. Q. Zhang, *Adv. Funct. Mater.* **2016**, *26*, 1233.
- [20] M. E. Levinstein, S. L. Rumyantsev, M. S. Shur, *Properties of Advanced Semiconductor Materials: GaN, AlN, InN, BN, SiC, SiGe*, Wiley, NY **2001**.
- [21] W. Chi, *Thermal Transport Properties of Thermally Sprayed Coatings: An Integrated Study of Materials, Processing and Microstructural Effects*, The Graduate School, Stony Brook University, Stony Brook, NY **2007**.
- [22] D. S. Jensen, S. S. Kanyal, V. Gupta, M. A. Vail, A. E. Dadson, M. Engelhard, R. Vanfleet, R. C. Davis, M. R. Linford, *J. Chromatogr. A* **2012**, *1257*, 195.
- [23] K. L. Stano, M. Carroll, R. Padbury, M. McCord, J. S. Jur, P. D. Bradford, *ACS Appl. Mater. Interfaces* **2014**, *6*, 19135.
- [24] J. Song, D. S. Jensen, D. N. Hutchison, B. Turner, T. Wood, A. Dadson, M. A. Vail, M. R. Linford, R. R. Vanfleet, R. C. Davis, *Adv. Funct. Mater.* **2011**, *21*, 1132.
- [25] A. Mahajerin, *Thin Film Encapsulation Methods for Large Area MEMS Packaging*, University of California, Berkeley, USA **2012**.
- [26] D. N. Hutchison, N. B. Morrill, Q. Aten, B. W. Turner, B. D. Jensen, L. L. Howell, R. R. Vanfleet, R. C. Davis, *J. Microelectromech. Syst.* **2010**, *19*, 75.
- [27] A. Chandrashekar, S. Ramachandran, G. Pollack, J.-S. Lee, G. S. Lee, L. Overzet, *Thin Solid Films* **2008**, *517*, 525.
- [28] N. Yazdani, V. Chawla, E. Edwards, V. Wood, H. G. Park, I. Utke, *Beilstein J. Nanotechnol.* **2014**, *5*, 234.
- [29] L. Acauan, A. C. Dias, M. B. Pereira, F. Horowitz, C. P. Bergmann, *ACS Appl. Mater. Interfaces* **2016**, *8*, 16444.
- [30] G. Fiorentino, S. Vollebregt, F. D. Tichelaar, R. Ishihara, P. M. Sarro, *Nanotechnology* **2015**, *26*, 064002.
- [31] A. Brieland-Shoultz, S. Tawfick, S. J. Park, M. Bedewy, M. R. Maschmann, J. W. Baur, A. J. Hart, *Adv. Funct. Mater.* **2014**, *24*, 5728.
- [32] H. Zhong, J. R. Lukes, *Phys. Rev. B* **2006**, *74*, 125403.
- [33] Z. Xu, M. J. Buehler, *ACS Nano* **2009**, *3*, 2767.
- [34] S. Sarkar, P. Das, *Rev. Adv. Mater. Sci.* **2014**, *37*, 53.
- [35] A. M. Marconnet, M. A. Panzer, K. E. Goodson, *Rev. Mod. Phys.* **2013**, *85*, 1295.
- [36] M. T. Pettes, L. Shi, *Adv. Funct. Mater.* **2009**, *19*, 3918.

- [37] T. Jeong, J.-G. Zhu, S. Mao, T. Pan, Y. J. Tang, *Int. J. Thermophys.* **2012**, *33*, 1000.
- [38] A. K. Roy, B. L. Farmer, V. Varshney, S. Sihn, J. Lee, S. Ganguli, *ACS Appl. Mater. Interfaces* **2012**, *4*, 545.
- [39] M. A. Panzer, G. Zhang, D. Mann, X. Hu, E. Pop, H. Dai, K. E. Goodson, *J. Heat Transfer* **2008**, *130*, 052401.
- [40] K. H. Baloch, N. Voskarian, J. Cumings, *Appl. Phys. Lett.* **2010**, *97*, 063105.
- [41] B. A. Cola, J. Xu, T. S. Fisher, *Int. J. Heat Mass Transfer* **2009**, *52*, 3490.
- [42] L. Wang, A. Bos, T. Van Weelden, F. Boschman, in *2010 11th Int. Conf. on Electronic Packaging Technology and High Density Packaging, (ICEPT-HDP 2010)*, IEEE, Xi'an, China **2010**, p. 55.
- [43] S. Kiwan, *Transp. Porous Media* **2007**, *67*, 17.
- [44] D. A. Nield, A. Bejan, *Convection in Porous Media*, Springer, New York, **2013**.
- [45] Y. Tian, C. Y. Zhao, *Nanosci. Nanotechnol. Lett.* **2011**, *3*, 769.
- [46] C. Silvestri, B. Morana, G. Fiorentino, S. Vollebregt, G. Pandraud, F. Santagata, G. Q. Zhang, P. M. Sarro, in *2014 IEEE 27th Int. Conf. on Micro Electro Mechanical Systems (MEMS)*, IEEE, San Francisco **2014**, p. 48.
- [47] B. Morana, G. Pandraud, J. F. Creemer, P. M. Sarro, *Mater. Chem. Phys.* **2013**, *139*, 654.
- [48] M. Riccio, A. Pantellini, A. Irace, G. Breglio, A. Nanni, C. Lanzieri, *Microelectron. Reliab.* **2011**, *51*, 1725.